Inorg. Chem. **2006**, *45*, 1595–1603

Transition State Characterization for the Reversible Binding of Dihydrogen to Bis(2,2'-bipyridine)rhodium(I) from Temperature- and Pressure-Dependent Experimental and Theoretical Studies

Etsuko Fujita,*,† Bruce S. Brunschwig,†,‡ Carol Creutz,† James T. Muckerman,† Norman Sutin,† David Szalda,§ and Rudi van Eldik£

Chemistry Department, Brookhaven National Laboratory, Upton, New York 11973-5000, and Institute for Inorganic Chemistry, University of Erlangen-Nürnberg, Egerlandstrasse 1, 91058 Erlangen, Germany

Received September 9, 2005

Thermodynamic and kinetic parameters for the oxidative addition of H_2 to $[Rh^{I}(bpy)_2]^+$ (bpy = 2,2′-bipyridine) to form $[Rh^{III}(H)_2(bpy)_2]^+$ were determined from either the UV–vis spectrum of equilibrium mixtures of $[Rh^{I}(bpy)_2]^+$ and $[Rh^{III}(H)_2(bpy)_2]^+$ or from the observed rates of dihydride formation following visible-light irradiation of solutions containing $[Rh^{III}(H)_2(bpy)_2]^+$ as a function of H_2 concentration, temperature, and pressure in acetone and methanol. The activation enthalpy and entropy in methanol are 10.0 kcal mol^{-1} and –18 cal mol^{-1} K^{-1}, respectively. The reaction enthalpy and entropy are –10.3 kcal mol^{-1} and –19 cal mol^{-1} K^{-1}, respectively. Similar values were obtained in acetone. Surprisingly, the volumes of activation for dihydride formation (–15 and –16 cm^3 mol^{-1} in methanol and acetone, respectively) are very close to the overall reaction volumes (–15 cm^3 mol^{-1} in both solvents). Thus, the volumes of activation for the reverse reaction, elimination of dihydrogen from the dihydrido complex, are approximately zero. B3LYP hybrid DFT calculations of the transition-state complex in methanol and similar MP2 calculations in the gas phase suggest that the dihydrogen has a short H–H bond (0.823 and 0.810 Å, respectively) and forms only a weak Rh–H bond (1.866 and 1.915 Å, respectively). Equal partial molar volumes of the dihydrogenrhodium(I) transition state and dihydridorhodium(III) can account for the experimental volume profile found for the overall process.

Introduction

Efforts to clarify the nature of the interaction of dihydrogen with low-valent metal centers and the formation of molecular dihydrogen complexes or high-valent dihydride complexes has attracted much attention.[1−8] We have previously investigated the oxidative addition of H_2 to $Rh^{I}(bpy)_2^+$ (bpy = 2,2′-bipyridine) to form the corresponding *cis*-dihydridorhodium(III) complex (eq 1).[9]

$$Rh^{I}(bpy)_2^+ + H_2 \underset{k_r}{\overset{k_f}{\rightleftharpoons}} cis\text{-}Rh^{III}(H)_2(bpy)_2^+ \qquad (1)$$

Irradiation (λ > 300 nm) of this reaction mixture results in the dissociation of the dihydrido complex and the formation of H_2 and $Rh^{I}(bpy)_2^+$, which is followed by the thermal relaxation of the perturbed system to re-form *cis*-$Rh^{III}(H)_2(bpy)_2^+$ when the light is extinguished. It was found that the observed pseudo-first-order rate constant for the relaxation process is given by eq 2, with k_f = 24.4 M^{-1} s^{-1} and k_r = 1.70 × 10^{-2} s^{-1} in acetone at 25 °C.[9]

* To whom correspondence should be addressed. E-mail: fujita@bnl.gov.
† Brookhaven National Laboratory.
‡ Permanent address: Molecular Material Research Center, Beckman Institute, MC 139−74, California Institute of Technology, Pasadena, CA 91125.
§ Permanent address: Department of Natural Sciences, Baruch College, New York, NY 10010.
£ University of Erlangen-Nürnberg.

(1) Kubas, G. *Acc. Chem. Res.* **1988**, *21*, 120−128.
(2) Crabtree, R. H. *Acc. Chem. Res.* **1990**, *23*, 95−101.
(3) Jessep, G.; Morris, R. H. *Coord. Chem. Rev.* **1992**, *121*, 155−284.
(4) Heinekey, D. M.; Oldham, W. J., Jr. *Chem. Rev.* **1993**, *93*, 913−926.
(5) Kubas, G. J. *Metal Dihydrogen and σ-Bond Complexes: Structure, Theory, and Reactivity*; Kluwer Academic/Plenum Publishers: New York, 2001.
(6) McGrady, G. S.; Guilera, G. *Chem. Soc. Rev.* **2003**, *32*, 383−392.
(7) Andrews, L. *Chem. Soc. Rev.* **2004**, *33*, 123−132.
(8) Heinekey, D. M.; Lledos, A.; Lluch, J. M. *Chem. Soc. Rev.* **2004**, *33*, 175−182.
(9) Yan, S. G.; Brunschwig, B. S.; Creutz, C.; Fujita, E.; Sutin, N. *J. Am. Chem. Soc.* **1998**, *120*, 10553−10554.

10.1021/ic0515498 CCC: $33.50
Published on Web 01/05/2006

$$k_{obs} = k_f[H_2] + k_r \quad (2)$$

The ratio of the rate constants, $k_f/k_r = 1.43 \times 10^3\ M^{-1}$, is in close agreement with the value of the equilibrium constant, $K_H = 1.45 \times 10^3\ M^{-1}$, obtained from equilibrium measurements.[9] Kinetic isotope effects for reductive elimination ($k_{r(H)}/k_{r(D)}$) and for oxidative addition ($k_{f(H)}/k_{f(D)}$) were reported to be 2.3 and 1.0, respectively.[9]

In the present work, we have extended our studies of this system as a function of temperature, pressure, and solvent in an effort to gain further insight into the nature of the transition state associated with the formation of the dihydrido complex. While the activation enthalpies ($\Delta H^{\ddagger}$) and entropies ($\Delta S^{\ddagger}$) and the reaction enthalpies (ΔH^0) and entropies (ΔS^0) for oxidative addition (or coordination) of hydrogen have been extensively investigated for a number of organometallic complexes,[5] there are few data for their activation ($\Delta V^{\ddagger}$) or reaction (ΔV^0) volumes. To our knowledge, no *reaction* volume data exist for oxidative addition reactions of H_2 to metal complexes. Only activation volumes at 10 °C for Vaska's complex, $IrCl(CO)(PPh_3)_2$, at 10 °C are known.[10] We have also restudied this reaction for comparison purposes. Activation and reaction volume data can be used to construct the volume changes that occur along the reaction coordinate for a particular reaction.[11] The poised $Rh^I(bpy)_2^+/Rh^{III}(H)_2(bpy)_2^+$ system is ideal for investigating both activation and equilibrium thermodynamic parameters experimentally. Here we report that the volume of activation for reaction 1 is approximately equal to the overall reaction volume, with the result that the back reaction exhibits almost no activation volume. B3LYP (i.e., Becke's three-parameter hybrid functional using the Becke exchange and the Lee−Yang−Parr correlation functionals) density functional theory (DFT) calculations including solvent effects on $Rh^I(bpy)_2^+$, $Rh^{III}(H)_2(bpy)_2^+$, and the transition-state (TS) complex were also carried out. These were supplemented with ab initio MP2 (Møller−Plesset second-order perturbation theory) calculations of all three species in the gas phase. The thermodynamic and mechanistic implications are discussed in detail.

Experimental Section

Materials. $[Rh^{III}(C_2O_4)(bpy)_2]ClO_4$ and $[Rh^I(bpy)_2]ClO_4$ were prepared as previously described.[12−14] $[Rh^I(bpy)_2]PF_6$ was obtained by reducing the Rh(III) complex with $NaBH_4$.[15] $IrCl(CO)(PPh_3)_2$ was purchased from Strem Chemicals, Inc. and used without purification. All complexes were characterized by UV−vis, IR, and NMR spectroscopy. ***(Warning:*** *The perchlorate salts used in this study may be explosive and are potentially hazardous.)*

Thermodynamic Measurements. For the equilibrium and kinetic studies at 25 °C, 0.01−1.0 mM solutions of $Rh^I(bpy)_2^+$ in acetone or methanol were prepared either by photochemical reduction of $[Rh^{III}(C_2O_4)(bpy)_2](ClO_4)$ or by dissolution of $[Rh^I(bpy)_2]PF_6$. Measurements were made using glass reaction vessels (total volume of 120 mL) directly attached to both 1 and 10 mm path length optical cells. Only the optical cell chamber containing an ~3 mL aliquot was thermostatically controlled. After a spectrum of $Rh^I(bpy)_2^+$ (1 mm optical cell) was recorded, an equilibrium mixture of $Rh^I(bpy)_2^+$ and $Rh^{III}(H)_2(bpy)_2^+$ was prepared by the addition of the desired amount of H_2 (with Ar added for a total pressure of 760 Torr). Spectra of the equilibrium mixture of $Rh^I(bpy)_2^+$ and $Rh^{III}(H)_2(bpy)_2^+$ (10 mm cell) were measured before and after all kinetic measurements to check for decomposition. For the kinetic measurements, the solutions were irradiated for 10 s using a 150 W xenon lamp equipped with a 300 nm long-path filter to liberate H_2 from the dihydrido complex. The disappearance of the photogenerated $Rh^I(bpy)_2^+$ was monitored with a HP 8452 A spectrophotometer (eq 1). Plots of the observed rate constants for the formation of $Rh^{III}(H)_2(bpy)_2^+$ as a function of the H_2 concentration were straight lines with slope and intercept of k_f and k_r, respectively.[9] The equilibrium constant (K_H) can also be obtained from the equilibrium concentrations of $Rh^I(bpy)_2^+$ and $Rh^{III}(H)_2(bpy)_2^+$.

$$K_H = \frac{[Rh^{III}(H_2)(bpy)_2^+]}{[Rh^1(bpy)_2^+][H_2]} \quad (3)$$

For the pressure- and temperature-dependent experiments, the solution containing $Rh^{III}(C_2O_4)(bpy)_2^+$ and H_2 was transferred by syringe to a gastight pillbox optical cell[16] that had been flushed with H_2. The pillbox was placed in a thermostated, four-window, high-pressure vessel[16] mounted in a HP 8452 A spectrophotometer. The photolysis of $Rh^{III}(C_2O_4)(bpy)_2^+$ to form a mixture of $Rh^I(bpy)_2^+$ and $Rh^{III}(H)_2(bpy)_2^+$ was performed in the pillbox cell within the high-pressure vessel while the solution was stirred with a glass-coated magnetic stirring bar. During syringe transfer of the solution to the pillbox cell, a small amount of dissolved H_2 escapes. Therefore, actual hydrogen concentrations were estimated from the observed rates at 25 °C using the k_{obs} vs $[H_2]$ data shown in Figure S1 (Supporting Information).

Toluene solutions of $Ir(H)_2Cl(CO)(PPh_3)_2$ were prepared by dissolving $IrCl(CO)(PPh_3)_2$ under a known concentration of H_2. The reaction rates for hydride formation were obtained with the same method used for $Rh^{III}(H)_2(bpy)_2^+$, except for a temperature of 35 °C.

Electronic Structure Calculations. B3LYP hybrid DFT and ab initio MP2 calculations on $Rh^I(bpy)_2^+$ and $Rh^{III}(H)_2(bpy)_2^+$ in the gas phase were carried out using D95V(d,p) (H,C,N,O)[17] and LANL2DZ ($n + 1$) ECP (Rh)[18,19] basis sets with the Gaussian 03 program.[20] To evaluate the solvation effect, we carried out B3LYP DFT calculations using the LACVP** basis set, consisting of 6-31G(d,p) (H,C,N,O)[21] and LANL2DZ ($n + 1$) ECP (Rh), with

(10) Schmidt, R.; Geis, M.; Kelm, H. *Z. Phys. Chem.* **1974**, *92*, 223.
(11) (a) van Eldik, R.; Dücker-Benfer, C.; Thaler, F. *Adv. Inorg. Chem.* **2000**, *49*, 1. (b) van Eldik, R.; Hubbard, C. D. In *High-Pressure Chemistry: Synthetic, Mechanistic and Supercritical Applications*; van Eldik, R., Klärner, F.-G., Eds.; VCH−Wiley, Weinheim, Germany, **2002**, p 3−40. (c) van Eldik, R.; Hubbard, C. D. In *Chemistry at Extreme Conditions*; Riad Manaa, M., Ed.; Elsevier: Amsterdam, 2005; Chapter 4. (d) Franke, A.; Stochel, G.; Jung, C.; van Eldik, R. *J. Am. Chem. Soc.* **2004**, *126*, 4181.
(12) Gillard, R. D.; De Jesus, J. P.; Sheridan, P. S. *Inorg. Synth.* **1980**, *20*, 58−60.
(13) Shinozaki, K.; Takahashi, N. *Inorg. Chem.* **1996**, *35*, 3917−3924.
(14) Chan, S. F.; Chou, M.; Creutz, C.; Matsubara, T.; Sutin, N. *J. Am. Chem. Soc.* **1981**, *103*, 369−379.
(15) Martin, B.; McWhinnie, W. R.; Waind, G. M. *J. Inorg. Nucl. Chem.* **1961**, *23*, 207−233.
(16) (a) le Noble, W. J.; Schlott, R. *Rev. Sci. Instrum.* **1976**, *47*, 770−771. (b) Spitzer, M.; Gärtig, F.; van Eldik, R. *Rev. Sci. Instrum.* **1988**, *59*, 2092.
(17) Dunning, T. H. J.; Hay, P. J. *Modern Theoretical Chemistry*; Plenum: New York, 1976; Vol. 3.
(18) (a) Hay, P. J.; Wadt, W. R. *J. Chem. Phys.* **1985**, *82*, 270−283. (b) Hay, P. J.; Wadt, W. R. *J. Chem. Phys.* **1985**, *82*, 299−310.
(19) Wadt, W. R.; Hay, P. J. *J. Chem. Phys.* **1985**, *82*, 284−298.

Table 1. Spectroscopic, Thermodynamic, and Kinetic Parameters for the Reaction of $Rh^{I}(bpy)_2^{+}$ with H_2 to Form $Rh^{III}(H)_2(bpy)_2^{+}$

solvent	methanol	acetone	DFT (B3LYP) calcd methanol	MP2 calcd gas phase
UV−vis spectrum of $Rh^{I}(bpy)_2^{+}$: λ_{max} (ϵ) (nm (mM^{-1} cm^{-1}))	246(24.5), 298(32.1), 362(6.8), 518sh(8.5), 552(13.1), 656sh(2.5), 750sh(0.5)	514sh(5.1), 552(12.5), 648(2.5), 750sh(0.5)		
k_f at 25 °C (M^{-1} s^{-1})	37 ± 2	28 ± 2		
k_r at 25 °C (s^{-1})	(1.5 ± 0.2) × 10^{-2}	(1.9 ± 0.3) × 10^{-2}		
k_f/k_r at 25 °C (M^{-1})	(2.5 ± 0.2) × 10^3	(1.5 ± 0.2) × 10^3 (3.4^a ± 0.2) × 10^3		
K_H at 25 °C (M^{-1})[b]	(2.7 ± 0.2) × 10^3	(2.0 ± 0.2) × 10^3		
$\Delta E°$ (kcal mol^{-1})			−6.3	−14.6
$\Delta H°$ (kcal mol^{-1})	−10.3 ± 0.4	−9.7 ± 0.5	−4.4 (−5.0)[c]	−12.0 (−12.6)[c]
ΔS^0 (cal mol^{-1} K^{-1})	−19 ± 2	−18 ± 2	−25 (−16)[c]	−25 (−16)[c]
ΔV^0 (cm^3 mol^{-1})	−15 ± 1	−15 ± 1		
$\Delta E_f^{\ddagger}$ (kcal mol^{-1})			12.1	12.1
$\Delta H_f^{\ddagger}$ (kcal mol^{-1})	10.0 ± 0.7	8.5 ± 0.7	11.7 (11.1)[c]	12.2 (11.6)[c]
$\Delta S_f^{\ddagger}$ (cal mol^{-1} K^{-1})	−18 ± 2	−23 ± 2	−26 (−17)[c]	−26 (−17)[c]
$\Delta V_f^{\ddagger}$ (cm^3 mol^{-1})	−16 ± 1	−15 ± 1, -14^a ± 1		
$\Delta H_r^{\ddagger}$ (kcal mol^{-1})	20.0 ± 0.7	18.1 ± 0.6	16.1 (16.1)[c]	24.2 (24.2)[c]
$\Delta S_r^{\ddagger}$ (cal mol^{-1} K^{-1})	0 ± 2	−6 ± 2	−1 (−1)[c]	−1 (−1)[c]

[a] With D_2 instead of H_2. [b] From spectroscopic equilibrium measurement, $K_H = [Rh^{III}(H)_2(bpy)_2^{+}]/[Rh^{I}(bpy)_2^{+}][H_2]$. [c] The experimental thermodynamic values are obtained relative to a 1 M concentration standard state. The theoretical values (i.e., 1 atm pressure standard state) are converted to a concentration standard state and shown in parentheses.

the Jaguar 5.5 program.[22] The effect of solvation was calculated using the self-consistent reaction field (SCRF) method as implemented in the Jaguar program. The Cartesian coordinates for $Rh^{I}(bpy)_2^{+}$, $Rh^{III}(H)_2(bpy)_2^{+}$, and the transition-state complex in MeOH, optimized at the B3LYP-DFT level of theory, are presented in Tables S1−S3 (Supporting Information). Time-dependent DFT (TDDFT) B3LYP calculations for $Rh^{I}(bpy)_2^{+}$ were carried out with the Gaussian 03 program to understand the electronic transition energies and excitations, as well as oscillator strengths.

Data Collection, Determination, and Refinement of the Crystal Structure. A black rod crystal (0.25 mm × 0.10 mm × 0.02 mm) of $Rh^{I}(bpy)_2^{+}$ obtained from CH_3CN was coated with perfluoropolyether and sealed inside a glass capillary. A wavelength of 0.956 Å was used, and the data were collected using image plates at the beam line X7B at the National Synchrotron Light Source (NSLS) at Brookhaven National Laboratory. The crystal exhibited monoclinic symmetry and systematic absences $0k0$, $k = 2n + 1$ and $h0l$, $h = 2n + 1$ consistent with the space group $P2_1/a$, a nonstandard setting of space group $P2_1/c$. Unit cell dimensions and other crystallographic information are reported in Table S4 (Supporting Information).

The structure was solved by standard heavy-atom Patterson methods. The asymmetric unit contains two formula units. Due to a limited data set and the quality of the crystal, the structure could only be refined to an R value of 15.7. The crystal also exhibited diffuse scattering.

Results

Reactivity of $Rh^{I}(bpy)_2^{+}$. $Rh^{I}(bpy)_2^{+}$ is stable in degassed acetone or methanol, showing an intense MLCT band at 552 nm. The spectrum shows additional shoulders between 450 and 750 nm, as summarized in Table 1. It is known[23] that aqueous solutions of $Rh^{I}(bpy)_2^{+}$ contain several species, including $[Rh^{I}(bpy)_2]_2^{2+}$, $Rh(H)(bpy)_2(H_2O)^{2+}$, and $[Rh(bpy)_2]_2H^{3+}$, depending on the total Rh concentration and pH of the solution. The spectra of the monomer, $Rh^{I}(bpy)_2^{+}$, and the dimer, $[Rh^{I}(bpy)_2]_2^{2+}$, have a λ_{max} of 505 and ∼530 nm, respectively, with very similar molar absorptivities (∼10^4 M^{-1} cm^{-1}, per Rh(I) center) at their respective maxima.[23] In acetone or methanol, no shift in the absorption maximum of the $Rh^{I}(bpy)_2^{+}$ is observed when the Rh(I) concentration is increased from 0.01 to 2 mM (the solubility limit). This indicates the existence of only the monomer in these solvents. Further, no spectral changes were observed with temperature between 10 and 40 °C. Two shoulders at 750 and 650 nm were observed in both methanol and acetone that were not previously reported for water or alcohol solutions.[23] Our TDDFT calculations predict that the transition at 750 nm corresponds to the HOMO-to-LUMO transition (see Theoretical Investigation).

Effects of H_2 Concentration and Temperature on the Formation of $Rh^{III}(H)_2(bpy)_2^{+}$. The UV−vis spectra of equilibrium mixtures of $Rh^{I}(bpy)_2^{+}$ and *cis*-$Rh^{III}(H)_2(bpy)_2^{+}$ were recorded as a function of $[H_2]$ at 25.0 °C. The solubility of H_2 in methanol and acetone under 1 atm pressure is 3.95 and 4.0 mM at 25 °C, respectively.[24,25] Assuming that only $Rh^{I}(bpy)_2^{+}$ absorbs at 552 nm (ϵ = 13.1 and 12.5 mM^{-1}

(20) Frisch, M. J.; Trucks, G. W.; Schlegel, H. B.; Scuseria, G. E.; Robb, M. A.; Cheeseman, J. R.; Montgomery, J. A., Jr.; Vreven, T.; Kudin, K. N.; Burant, J. C.; Millam, J. M.; Iyengar, S. S.; Tomasi, J.; Barone, V.; Mennucci, B.; Cossi, M.; Scalmani, G.; Rega, N.; Petersson, G. A.; Nakatsuji, H.; Hada, M.; Ehara, M.; Toyota, K.; Fukuda, R.; Hasegawa, J.; Ishida, M.; Nakajima, T.; Honda, Y.; Kitao, O.; Nakai, H.; Klene, M.; Li, X.; Knox, J. E.; Hratchian, H. P.; Cross, J. B.; Bakken, V.; Adamo, C.; Jaramillo, J.; Gomperts, R.; Stratmann, R. E.; Yazyev, O.; Austin, A. J.; Cammi, R.; Pomelli, C.; Ochterski, J. W.; Ayala, P. Y.; Morokuma, K.; Voth, G. A.; Salvador, P.; Dannenberg, J. J.; Zakrzewski, V. G.; Dapprich, S.; Daniels, A. D.; Strain, M. C.; Farkas, O.; Malick, D. K.; Rabuck, A. D.; Raghavachari, K.; Foresman, J. B.; Ortiz, J. V.; Cui, Q.; Baboul, A. G.; Clifford, S.; Cioslowski, J.; Stefanov, B. B.; Liu, G.; Liashenko, A.; Piskorz, P.; Komaromi, I.; Martin, R. L.; Fox, D. J.; Keith, T.; Al-Laham, M. A.; Peng, C. Y.; Nanayakkara, A.; Challacombe, M.; Gill, P. M. W.; Johnson, B.; Chen, W.; Wong, M. W.; Gonzalez, C.; Pople, J. A. *Gaussian 03*, revision B.04; Gaussian, Inc.: Wallingford, CT, 2004.
(21) (a) Hariharan, P. C.; Pople, J. A. *Theor. Chim. Acta* **1973**, *28*, 213. (b) Francl, M. M.; Petro, W. J.; Hehre, W. J.; Binkley, J. S.; Gordon, M. S.; DeFrees, D. J.; Pople, J. A. *J. Chem. Phys.* **1982**, *77*, 3654.
(22) *Jaguar 5.0*; Schrödinger, LLC: Portland, OR.
(23) Chou, M.; Creutz, C.; Mahajan, D.; Sutin, N.; Zipp, A. P. *Inorg. Chem.* **1982**, *21*, 3989−3997.
(24) Fogg, P. G. T.; Gerrard, W. *Solubility of Gases in Liquids*; Wiley: Chichester, 1991.

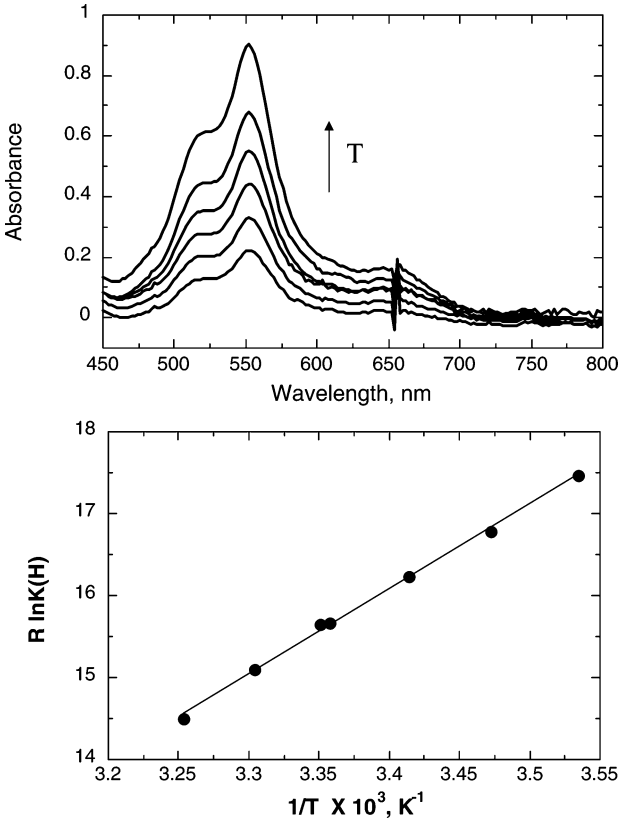

Figure 1. (Top) Temperature-dependent spectra of the equilibrium mixture of $Rh^{I}(bpy)_2^+$ and $Rh^{III}(H)_2(bpy)_2^+$ in methanol at 9.9, 15.0, 19.9, 25.2, 29.7, and 34.4 °C. The higher the temperature, the more $Rh^{I}(bpy)_2^+$ exists. (Bottom) Plot of $\ln(K_H)$ versus $1/T$ from which $\Delta H^0 = -10.3 \pm 0.4$ kcal mol^{-1} and $\Delta S^0 = -19 \pm 2$ cal mol^{-1} K^{-1} were obtained.

cm^{-1} in methanol and acetone, respectively), the equilibrium constant can be calculated from $K_H = (A_0 - A)/[H_2]A$ where A_0 and A are the absorbances prior to and after addition of H_2 (see eqs 1 and 3). Values for K_H of $(2.7 \pm 0.2) \times 10^3$ and $(2.0 \pm 0.2) \times 10^3$ M^{-1} in methanol and acetone, respectively, were obtained. The value obtained in acetone is slightly larger than that previously reported[9] of 1.45×10^3 M^{-1} at 25 °C.

The forward and reverse rate constants for reaction 1 in methanol and acetone were determined as a function of H_2 concentration. Figure S1 (Supporting Information) shows the observed rate constants for the formation of $Rh^{III}(H)_2(bpy)_2^+$ in methanol. The slope and the intercept of the plot yield $k_f = 37 \pm 1.5$ M^{-1} s^{-1} and $k_r = (1.5 \pm 0.2) \times 10^{-2}$ s^{-1}. Similar experiments in acetone yield $k_f = 28 \pm 2$ M^{-1} s^{-1} and $k_r = (1.9 \pm 0.3) \times 10^{-2}$ s^{-1}, close to the values reported previously ($k_f = 24.4$ M^{-1} s^{-1} and $k_r = 1.70 \times 10^{-2}$ s^{-1}).[9] The equilibrium constants calculated from k_f/k_r in methanol and acetone are $(2.5 \pm 0.2) \times 10^3$ and $(1.5 \pm 0.2) \times 10^3$ M^{-1}, respectively, and are consistent with the values obtained from the spectroscopic measurements.

The UV−vis spectra of equilibrium mixtures of $Rh^{I}(bpy)_2^+$ and *cis*-$Rh^{III}(H)_2(bpy)_2^+$ were recorded as a function of temperature in methanol (Figure 1) and in acetone. When the temperature is increased, the intensity of the peak at 552 nm increases due to a shift in equilibrium toward $Rh^{I}(bpy)_2^+$, thus indicating that reaction 1 is exothermic. From the slope and the intercept of a plot of $\ln(K_H)$ versus $1/T$ (Figure 1, bottom) and eq 4, where R is the gas constant, we obtained $\Delta H^0 = -10.3 \pm 0.4$ kcal mol^{-1} and $\Delta S^0 = -19 \pm 2$ cal mol^{-1} deg^{-1}.

$$R \ln(K_H) = -\frac{\Delta H^0}{T} + \Delta S^0 \qquad (4)$$

The temperature dependence of the rate of oxidative addition of H_2 to photogenerated $Rh^{I}(bpy)_2^+$ was studied by UV−vis spectroscopy by monitoring the decay of the $Rh^{I}(bpy)_2^+$ absorption under a known pressure of H_2 in the temperature range 10−35 °C using a gastight pillbox cell. The activation parameters ($\Delta H_f^{\ddagger}$, $\Delta S_{f\ddagger}$, $\Delta H_r^{\ddagger}$, and $\Delta S_r^{\ddagger}$) in methanol and acetone were obtained from the slope ($\Delta H_f^{\ddagger}$ and $\Delta H_r^{\ddagger}$) and the intercept ($\Delta S_f^{\ddagger}$ and $\Delta S_r^{\ddagger}$) of the plots (shown in Figure S2a and b, Supporting Information) using eqs 5 and 6, where h is Planck's constant and k_B is Boltzmann's constant. The results are summarized in Table 1.

$$R \ln\left(\frac{hk_{obs}K_H}{k_B T(K_H[H_2] + 1)}\right) = -\frac{\Delta H_f^{\ddagger}}{T} + \Delta S_f^{\ddagger} \qquad (5)$$

$$R \ln\left(\frac{hk_{obs}}{k_B T(K_H[H_2] + 1)}\right) = -\frac{\Delta H_r^{\ddagger}}{T} + \Delta S_r^{\ddagger} \qquad (6)$$

The activation enthalpy and entropy for the forward reaction are 10 kcal mol^{-1} and ≈ -20 cal mol^{-1} K^{-1}, respectively.

To make the comparison of experimental enthalpies and theoretical activation and reaction parameters, it is necessary to recognize that the standard state for H_2 employed in the theory is 1 atm pressure while that in the current experiment is 1 M. The correction for this change in the standard states is given in the Supporting Information.

Effects of Pressure on the Formation of $[Rh^{III}(H)_2(bpy)_2]^+$. UV−vis spectra of an equilibrium mixture of $Rh^{I}(bpy)_2^+$ and *cis*-$Rh^{III}(H)_2(bpy)_2^+$ were recorded as a function of pressure at 25 °C. With an increase in pressure, the reaction shifts to the right and the absorbance at 552 nm ($Rh^{I}(bpy)_2^+$) decreases, as shown in Figure 2a for methanol. Thus, increasing pressure favors product formation, $Rh^{III}(H)_2(bpy)_2^+$, while increasing temperature favors the reactants, H_2 and $Rh^{I}(bpy)_2^+$. The spectral changes observed on changing the pressure were reversible and were used to calculate the value of K_H as function of pressure. A plot of $\ln(K_H)$ versus pressure is significantly curved, Figure 2b, i.e., the reaction volume, ΔV^0 calculated from the slope ($= -\Delta V^0/RT$) of the line decreases with increasing pressure. This effect is due to the compressibility of the solvent. To determine the reaction volume at ambient conditions, the data were fit with a parabolic function (eq 7),[11c]

$$\ln(K_H) = a + bP + cP^2 \qquad (7)$$

and the initial slope was used to calculate the reaction volume from eq 8,

(25) Young, C. L. *Hydrogen and Deuterium*; Pergamon Press: Oxford, 1982; Vol. 5/6.

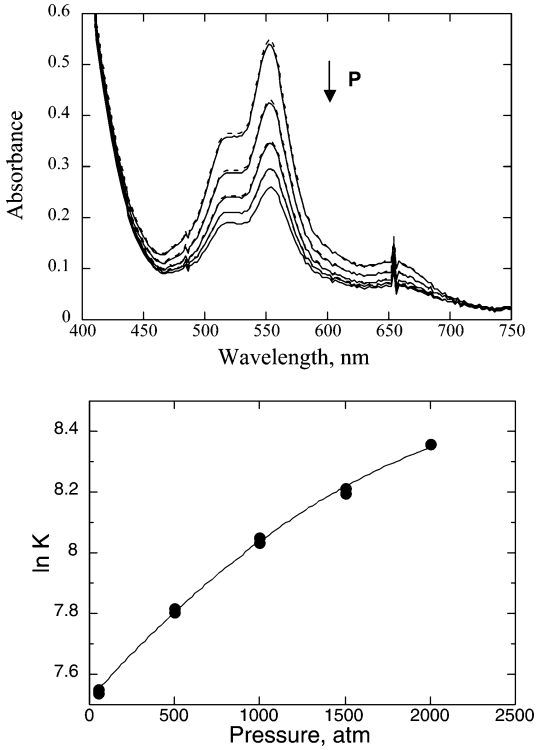

Figure 2. Pressure dependence of the equilibrium constant for reaction 1 in methanol; top: the spectral change observed on changing the pressure 50, 500, 1000, 1500, and 2000 atm (solid lines), then 1500, 1000, 500, and 50 atm (dashed lines). The intensity of the band at 552 nm decreases with increasing pressure; bottom: a plot of $\ln(K_H)$ vs pressure.

$$b = -\frac{\Delta V^0}{RT} \tag{8}$$

This yields $\Delta V^0 = -15 \pm 1$ cm^3 mol^{-1} in both methanol (shown in Figure 2b) and acetone.

The forward rate constants for reaction 1 in methanol and acetone were determined under various pressures at 25 °C. Since under our conditions $k_f[H_2] \gg k_r$, the limiting form $k_{obs} \approx k_f[H_2]$ can be used. The effect of pressure on the relaxation process was found to be reproducible for a complete pressure cycle, i.e., increasing the pressure stepwise from ambient to 2000 atm and then decreasing the pressure stepwise back to ambient conditions. A plot of $\ln(k_{obs})$ versus pressure in methanol is shown in Figure 3. The activation volume (viz. -16 cm^3 mol^{-1}) was estimated from the initial slope of the plot ($b = -\Delta V^{\ddagger}/RT$). The results are summarized in Table 1 and Figure 4.

Effects of Pressure on the Formation of Ir(H)$_2$Cl(CO)(PPh$_3$)$_2$. Reaction rates for oxidative addition of H_2 to IrCl(CO)(PPh$_3$)$_2$ in toluene were obtained using the same method as used for Rh^{III}(H)$_2$(bpy)$_2^+$. Because oxidative addition of H_2 to IrCl(CO)(PPh$_3$)$_2$ is much slower than for that of Rh^{I}(bpy)$_2^+$, the former reaction was studied at 35 °C. Figure S3 shows the spectral changes of IrCl(CO)(PPh$_3$)$_2$ to form Ir(H)$_2$Cl(CO)(PPh$_3$)$_2$ at 2 min intervals under 1 atm H_2 at 35 °C. From a plot of $\ln(k_{obs})$ versus pressure in toluene (Figure S4), the activation volume of -20 ± 1 cm^3 mol^{-1} was obtained for reaction with both H_2 and D_2.

Structure of [Rh^{I}(bpy)$_2$](ClO$_4$). Selected bond lengths and angles (Table 2), an ORTEP drawing showing the atom numbering (Figure S5a), crystal data and structure refinement (Table S4), and CIF files are given as Supporting Information.

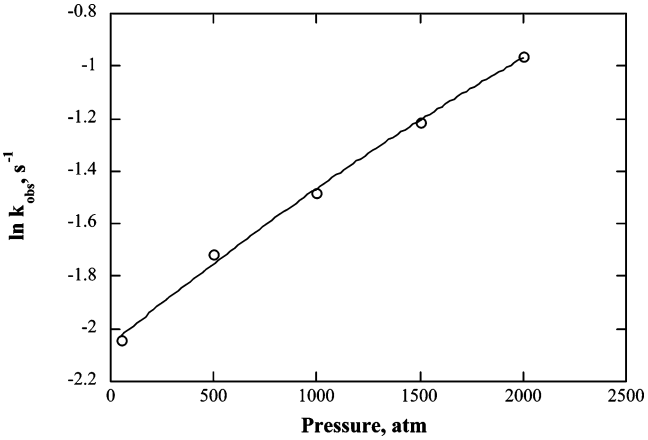

Figure 3. Pressure dependence of the rate constant for formation of Rh^{III}(H)$_2$(bpy)$_2^+$ in methanol according to reaction 1.

In each complex in the asymmetric unit, the rhodium atom is coordinated by the nitrogen atoms of two bidentate bipyridine ligands. The formula unit also contains a perchlorate anion and two acetonitrile molecules of crystallization. The average Rh−N bond distance is 2.01 Å. The coordination sphere about the rhodium has a tetrahedrally distorted square-planar geometry. The nitrogen atoms of the two bipyridine ligands are 0.32 and 0.23 Å out of the least-squares plane formed by the four nitrogen atoms and the rhodium atom. The least-squares planes between the two bipyridine ligands within a complex form angles of 40.1° and 39.8° with one another. Within the bipyridine ligand, the two pyridine rings are folded forming angles of 13.8°, 15.9° and 14.1°, 12.3°. Thus, to relieve the steric crowding of the two bipyridine rings, the coordination sphere has a tetrahedral distortion and the bipyridine rings are bent (see Figure S5a and b, Supporting Information). The rhodium complexes are stacked in infinite chains along the crystallographic 2-fold screw axis with a Rh−Rh distance of 3.64 Å with eclipsing bipyridines rings, as shown in Figure S5b. The two crystallographically independent chains are almost identical.

Theoretical Investigation. Quantum mechanical calculations were used to predict the structure of Rh^{III}(H)$_2$(bpy)$_2^+$, Rh^{I}(bpy)$_2^+$, and the transition state for the oxidative addition of H_2. Initial gas-phase DFT calculations[26−28] on Rh^{I}(bpy)$_2^+$ and Rh^{III}(H)$_2$(bpy)$_2^+$ were carried out using the Gaussian 03 program.[20] Preliminary geometry optimizations were performed for both rhodium complexes without symmetry constraints. From these results, it became clear that Rh^{I}(bpy)$_2^+$ adopts a structure of D_2 symmetry while Rh^{I}(bpy)$_2$(H)$_2^+$ and the Rh^{I}(bpy)$_2$(H$_2$) TS complex (see below) adopt a structure of C_2 symmetry. The structures were then re-optimized with the appropriate symmetry constraints. Also, gas-phase MP2 and solvent-phase DFT calculations were

(26) Becke, A. D. *Phys. Rev. A* **1988**, *38*, 3098.
(27) Lee, C.; W., Y.; Parr, R. G. *Phys. Rev. B* **1988**, *37*, 785.
(28) Miehlich, B.; Savin, A.; Stoll, H.; Preuss, H. *Chem. Phys. Lett.* **1989**, *157*, 200.

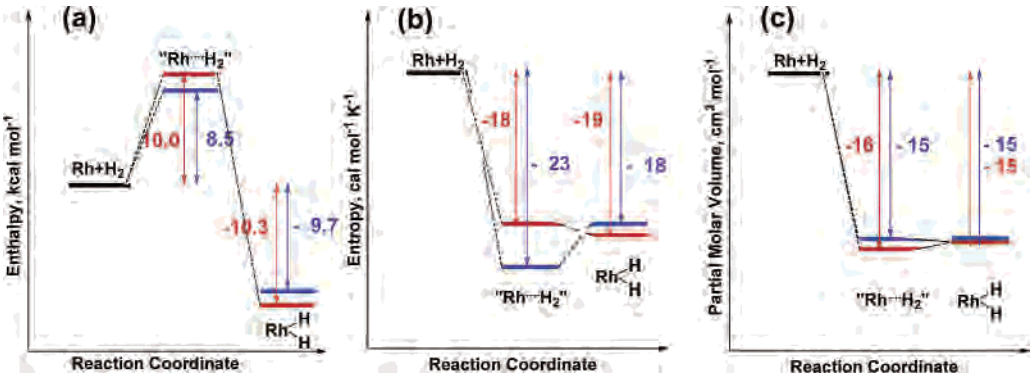

Figure 4. Experimental energy, entropy, and volume profiles for the oxidative addition of H_2 to $Rh^I(bpy)_2^+$ in methanol (red) and acetone (blue): (a) enthalpy, (b) entropy, and (c) partial molar volume.

Table 2. Experimental and Theoretical Bond Lengths [Å] and Angles [deg] for $Rh^I(bpy)_2^+$

	X-ray structure[a]	DFT (B3LYP) calcd gas phase	DFT (B3LYP) calcd methanol	MP2 calcd gas phase
Rh−N	2.01	2.069	2.093	2.014
N−C2	1.38	1.365	1.366	1.373
C2−C3	1.38	1.401	1.398	1.404
C3−C4	1.38	1.396	1.393	1.398
C4−C5	1.41	1.400	1.395	1.405
C5−C6	1.40	1.395	1.391	1.397
C6−N	1.35	1.350	1.350	1.361
C2−C2′	1.49	1.473	1.472	1.466
N−Rh−N[b]	78.6	78.6	78.0	79.5
N−Rh−N[c]	103.4	104.1	104.5	103.4
N−Rh−N[d]	164.6	162.8	163.2	161.8
Rh−N−C2	118	115.7	115.6	116.2
N−C2−C3	124	121.7	121.4	121.9
C2−C3−C4	121	119.7	119.6	119.7
C3−C4−C5	118	118.5	118.8	118.4
C4−C5−C6	116	118.8	118.8	119.2
C5−C6−N	127	123.2	122.9	122.9
C6−N−C2	113	118.1	118.4	117.8
C6−N−Rh	127	125.0	124.8	124.5
N−C2−C2′	112	114.6	114.9	113.6
C2′−C2−C3	124	123.7	123.6	124.4

[a] Averaged bond length. [b] Both N atoms in one bpy. [c] N atoms in the different bpy ligands. [d] N atoms located in the trans position.

performed. Table 2 lists the principal geometric properties of the optimized $Rh^I(bpy)_2^+$ complex in the gas phase and in methanol, together with X-ray crystal data. Table 3 shows the geometric properties of the optimized $Rh^{III}(H)_2(bpy)_2^+$ and the transition-state complex. Figure 5 shows the optimized structures of $Rh^I(bpy)_2^+$, $Rh^{III}(H)_2(bpy)_2^+$, and the TS complex in the gas phase at the B3LYP level of theory.

The geometry-optimized DFT (B3LYP) structure of $Rh^I(bpy)_2^+$ is very similar to that of the single-crystal structure, Table 2. While the observed Rh−N distances are slightly longer for the DFT-calculated (0.06 and 0.08 Å longer for the gas phase and methanol, respectively), they are very close for the MP2 calculation. The coordination sphere around Rh has a tetrahedrally distorted square-planar geometry, as observed. The planes between the two bipyridine ligands form angles of 42° with one another.

The DFT (B3LYP) coordination geometries in $Rh^{III}(H)_2(bpy)_2^+$ in the gas phase and in methanol and the MP2 coordination geometry are all similar, as shown in Table 3. The distances within the bpy ligand are all similar. The H−H distance in the MP2 structure is 0.1 Å shorter than that in the DFT structures. The geometry around Rh is approximately octahedral with a H−Rh−H angle of ≈83 ± 2°. The B3LYP Rh−N bond distances perpendicular to the plane made by H−Rh−H in the gas phase and methanol are 2.064 and 2.081 Å, respectively, and the others are 2.235 and 2.226 Å, respectively. The long bond distances observed in all structures are due to the trans effect of the Rh−H bond. The tendency of MP2 calculation to yield shorter bond distances than those obtained from DFT calculations is as expected.[29]

The B3LYP gas-phase geometry of the TS complex was calculated by the same method used for the stable complexes. The optimized geometries (C_2 symmetry) of the TS complex in the gas phase (B3LYP and MP2) and in methanol (B3LYP) are similar, as shown in Table 3. As can be seen from Figures 5 and S6a, the geometry around the Rh is not octahedral, but rather it is closer to a five-coordinate side-on H_2 complex with a H−Rh−H angle of ≈25°. The H_2 axis is not aligned with one N−Rh−N plane but is rotated slightly (Figure S6b). The Rh−N distance perpendicular to the H−Rh−H plane is 2.068 Å, and the other Rh−N distance is 2.196 Å in methanol. The Rh−H distance in general is long at 1.88 Å (compared to 1.55 Å for $Rh^{III}(H)_2(bpy)_2^+$), and the H−H distance is very short at 0.82 Å (close to 0.74 Å for free dihydrogen). The TS complex can be characterized as a dihydrogen-like complex. The dihedral angles between two least-squares planes of the bpy ligands are ≈42°, 86°, and 58° for $Rh^I(bpy)_2^+$, $Rh^{III}(H)_2(bpy)_2^+$, and the TS complex, respectively. The MP2 structure is similar to the B3LYP structures except that the Rh−N distances are slightly shorter. While the MP2 calculations were useful in corroborating the geometrical properties of the various Rh complexes studied here, the primary reason for carrying them out was to obtain a better theoretical estimate of the energetics of activation and reaction.

Thermodynamic parameters (1 atm pressure standard state) obtained from the B3LYP and MP2 calculations are shown together with those relative to a 1 M concentration standard state in parentheses in Table 1 (see the correction in the Supporting Information). Previous calculations on rhenium bipyridine complexes[29] indicated that the B3LYP relative energetics were not accurate to better than 4−6 kcal mol^{-1},

(29) Fujita, E.; Muckerman, J. T. *Inorg. Chem.* **2004**, *43*, 7636−7647.

Table 3. Selected Calculated Bond Lengths [Å] and Angles [deg] for $Rh^{III}(H)_2(bpy)_2^+$ and the TS Complex

	$Rh^{III}(H)_2(bpy)_2^+$ DFT (B3LYP) calcd gas phase	$Rh^{III}(H)_2(bpy)_2^+$ DFT (B3LYP) calcd methanol	$Rh^{III}(H)_2(bpy)_2^+$ (MP2) gas phase	TS complex DFT (B3LYP) calcd gas phase	TS complex DFT (B3LYP) calcd methanol	TS complex MP2 gas phase
Rh−H	1.550	1.553	1.537	1.887	1.866	1.915
H−H	2.034	2.109	1.992	0.817	0.823	0.810
Rh−N	2.064, 2.235	2.081, 2.226	2.028, 2.179	2.053, 2.172	2.068, 2.196	2.009, 2.072
H−Rh−H	82.1	85.5	80.8	25.0	25.5	24.4

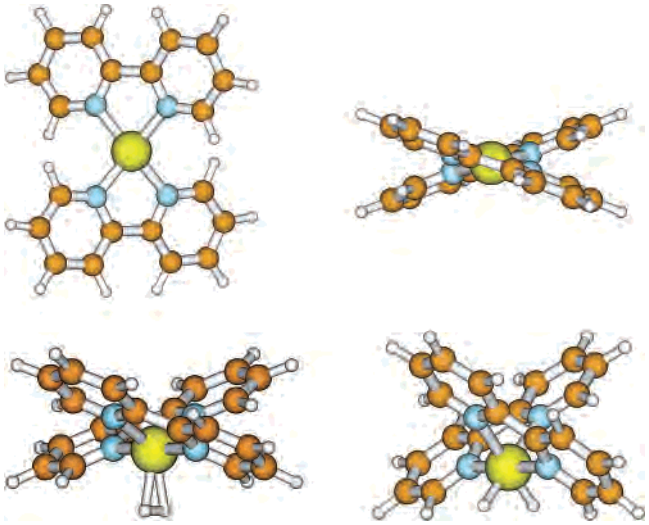

Figure 5. Calculated gas-phase structures of $Rh^I(bpy)_2^+$ (top two structures), the TS complex (bottom left), and $Rh^{III}(H)_2(bpy)_2^+$ (bottom right) at the DFT (B3LYP) gas-phase level of theory.

while MP2 calculations could account for the observed conformer of the dimer skewed-*cis*-$[Re(bpy)(CO)_3]_2$. Indeed, in the present work, the calculated B3LYP energetics (in the concentration standard) in methanol are in some disagreement with the observed reaction exothermicity (−5.0 vs −10.3 kcal mol^{-1} in methanol, see Table 1) but are in good agreement with the activation enthalpy (11.1 vs 10.0 kcal mol^{-1} in methanol). The gas-phase MP2 results, using the calculated B3LYP vibrational frequencies to compute zero-point energy and thermal effects, are in reasonably good agreement with both reaction (−12.6 kcal mol^{-1}) and activation (11.6 kcal mol^{-1}) enthalpies. The difference in solvation energies for reaction (−1.7 kcal mol^{-1}) and activation (1.1 kcal mol^{-1}) in the B3LYP calculations in methanol, if added to the gas-phase MP2 results, would make the discrepancies larger. The discrepancies are likely due to the fact that many of the vibrational frequencies are too low to be treated in the harmonic approximation.

In both $Rh^I(bpy)_2^+$ and $Rh^{III}(H)_2(bpy)_2^+$, the HOMOs are metal-based orbitals and the LUMOs are bpy-based orbitals. The frontier orbitals of $Rh^I(bpy)_2^+$ are shown in Figure 6. Table 4 summarizes the observed and calculated (TDDFT) transitions for $Rh^I(bpy)_2^+$ in methanol. The TDDFT calculations predict that the lowest-energy transition of $Rh^I(bpy)_2^+$ is the HOMO-to-LUMO excitation at 777 nm with an oscillator strength of 0.0016 while the strongest is the HOMO−2-to-LUMO at 533 nm with an oscillator strength of 0.1867. The HOMO, HOMO−1, and HOMO−2 are all predominately metal centered, while the LUMO, LUMO+1, and LUMO+2 are mainly bpy π^* in character. Thus, we may characterize all of these as MLCT transitions except the transition at 441 nm, where the d_{z^2}-to-d_{xy} character cannot be totally ignored. The predicted and observed transitions and relative intensities are in excellent agreement, except for the shoulder observed at ≈520 nm.

The orbital interactions between molecular hydrogen and $Rh^I(bpy)_2^+$ are reflected in the orbitals of the transition state for the oxidative addition of H_2. The HOMO of the transition state is essentially the antibonding combination of the d_{z^2} HOMO of $Rh^I(bpy)_2^+$ with the σ-bonding orbital of H_2. The bonding combination of the metal d_{z^2} and H_2 σ-bonding orbital is of much lower energy and contributes two partial metal−hydrogen bonds. The HOMO−1 of the transition state corresponds to the bonding combination of the d_{xz} HOMO−1 of $Rh^I(bpy)_2^+$ and the σ^* antibonding orbital of H_2 (resulting in two additional partial metal−hydrogen bonds). The net result is two partial metal−hydrogen bonds and a weakened H−H bond in the transition state.

Discussion

The spectroscopic behavior of $Rh^I(bpy)_2^+$ in alcohol and water has been extensively studied.[23] In water at high pH, the tetrahedrally distorted square-planar $Rh^I(bpy)_2^+$ complex (λ_{max} = 505 nm) and the dimer with a weak Rh−Rh interaction (λ_{max} = 530 nm) are present at low and high total Rh(I) concentrations, respectively.[23] Rh−Rh bond formation between d^8 complexes is well-known, and in the crystal, the $Rh^I(bpy)_2^+$ complexes are stacked in infinite chains along the crystallographic 2-fold screw axis with a Rh−Rh distance of 3.64 Å with eclipsing bipyridine rings (Figure S5b). We have observed weak absorption bands (i.e., shoulders) around 650 and 750 nm in acetone and methanol that were not previously observed in water or alcohol.[23] The time-dependent B3LYP calculations on $Rh^I(bpy)_2^+$ predict that the lowest-energy transition is the HOMO-to-LUMO excitation at 777 nm (Table 4). We therefore assign the observed 750 nm absorption (rather than the 505 nm transition as previously assigned in water)[23] to the lowest-energy MLCT transition. In general, the predicted transitions and relative intensities are in good agreement with the experimental UV−vis spectrum (Table 4); however, the assignment of a shoulder around 520 nm near the strongest absorption at 550 nm is not clear. The three weak absorptions predicted around 440 nm are unlikely to account for the 520 nm shoulder. Alternatively, solvent bonding to form a five-coordinate (or six-coordinate) species could shift the 550 nm band to higher energy. Supporting this suggestion, we observe that the shoulder around 520 nm is more pronounced in methanol than in acetone.

Figure 4 indicates thermodynamic profiles (i.e., enthalpy, entropy, and partial molar volume change) for the oxidative

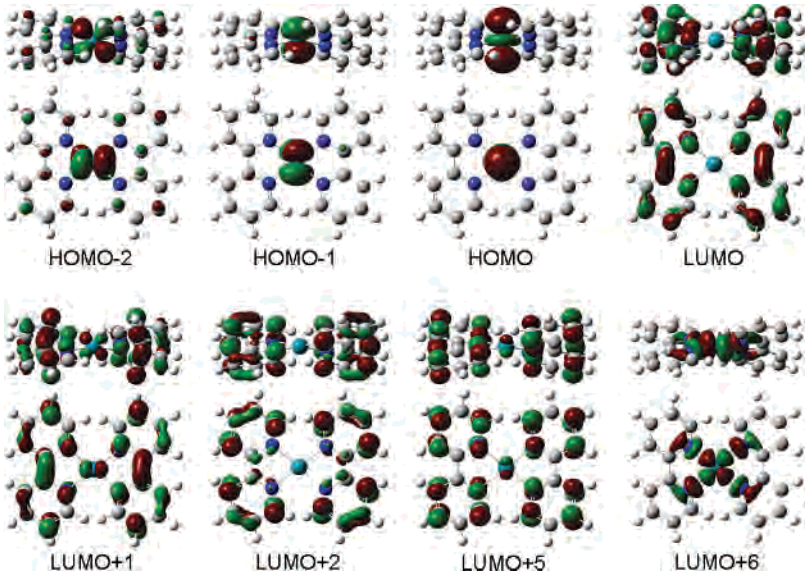

Figure 6. Frontier orbitals for $Rh^{I}(bpy)_2^+$: viewed parallel to the average plane made by Rh and four nitrogen atoms (top) and perpendicular to the average plane (bottom) from gas-phase B3LYP calculations.

Table 4. Observed and Calculated Visible Transitions for $Rh^{I}(bpy)_2^+$ in Methanol and the Gas Phase, Respectively

observed transitions		calculated transitions		
λ_{max} (ϵ) nm (mM^{-1} cm^{-1})	orbital assignment	transition character	λ_{max} nm	oscillator strength
750sh (0.5)	HOMO to LUMO	d_{z^2} to bpy π^*	777	0.0016
656sh (2.5)	HOMO−1 to LUMO	d_{yz} to bpy π^*	634	0.0063
552 (13.1)	HOMO−2 to LUMO	d_{xz} to bpy π^*	533	0.1867
518sh (8.5)				
	HOMO to LUMO+2	d_{z^2} to bpy π^*	447	0.0013
	HOMO to LUMO+6	d_{z^2} to (d_{xy} and bpy π^*)	441	0.0013
	HOMO to LUMO+5	d_{z^2} to bpy π^*	423	0.0024
362 (6.8)	HOMO−1 to LUMO+2	d_{yz} to bpy π^*	397	0.0062

addition of H_2 to $Rh^{I}(bpy)_2^+$ (eq 1) in methanol (red line) and acetone (blue line). The differences in the values obtained in methanol and acetone are small (Table 1). The heats of formation and activation energies calculated with the B3LYP and MP2 methods for formation of $Rh^{III}(H)_2(bpy)_2^+$ are also given in Table 1. The MP2 calculated values for ΔH^0 and $\Delta H_f^{\ddagger}$ are in reasonable agreement with the experimental values.

The negative values of the experimental reaction and activation entropies are consistent with an associative reaction. However, it is surprising that the activation volumes in methanol and acetone are very similar to the overall reaction volumes (within 1 cm^3 mol^{-1}, Table 1), indicating that the activation volume for the reverse reaction, elimination of dihydrogen from the dihydrido complex, is practically zero. In general, oxidative addition reactions are expected to be accompanied by significant volume changes. Such reactions involve not only significant bond formation in reaching the transition state but also a change in the oxidation state and coordination number of the metal complex. These effects are expected to cause significant reaction volume contraction (over -20 cm^3 mol^{-1}), such that these reactions should exhibit a rather large pressure sensitivity. On the basis of activation volumes reported in the literature for typical oxidative addition and reductive elimination reactions[10,11] and reaction volumes reported for the interaction of Co(I) complexes with CO_2 and weak acids during which Co(III) complexes are formed,[30,31] significant volume effects are to be expected for both the forward and back reactions in eq 1.

The partial molar volumes of H_2 are 26.7, 38, and 35 cm^3 mol^{-1} in water, acetone, and methanol, respectively.[32−34] There are few data on the activation volumes for oxidative addition of H_2 to metal complexes. The activation volume for oxidative addition of dihydrogen to *trans*-[Ir(CO)Cl-$(PPh_3)_2$] has been reported to be -19 ± 1 cm^3 mol^{-1} in DMF, chlorobenzene, or toluene at 10 °C measured by a conventional mixing method.[10] As shown in Figure S4, we obtained -20 ± 1 cm^3 mol^{-1} in toluene at 35 °C for the oxidative addition of either H_2 or D_2 to $IrCl(CO)(PPh_3)_2$ using the same method used for $Rh^{I}(bpy)_2^+$. The observed volume of activation for the binding of dihydrogen to $IrCl(CO)(PPh_3)_2$ is ≈30% more negative than those found for the binding to $[Rh^{I}(bpy)_2]^+$ of ≈ -15 cm^3 mol^{-1} in methanol or acetone. Unfortunately, the overall reaction volume, ΔV^0, for the oxidative addition of H_2 to $IrCl(CO)(PPh_3)_2$ could not be determined, owing to the large equilibrium constant of that reaction.

(30) Fujita, E.; van Eldik, R. *Inorg. Chem.* **1998**, *37*, 360−362.
(31) Fujita, E.; Wishart, J. F.; van Eldik, R. *Inorg. Chem.* **2002**, *41*, 1779−1583.
(32) Hildebrand, J. H.; Scott, R. L. *Solutions of Non-Electolytes*; Reinhold Publishing Corporation: New York, 1950.
(33) Pierotti, R. A. *J. Phys. Chem.* **1965**, *69*, 281−288.
(34) Moore, J. C.; Battino, R.; Rettich, T. R.; Handa, Y. P.; Wilhelm, E. *J. Chem. Eng. data* **1982**, *27*, 22−24.

Volumes of reaction and activation can be estimated using the structures of the reactants, transition state, and products. We have used both DFT and ab initio quantum calculations to obtain the structures of $Rh^{I}(bpy)_2^+$, $Rh^{III}(H)_2(bpy)_2^+$, and the TS species. The structures obtained for the $Rh(bpy)_2^+$ are in good agreement with the observed crystal structure (Table 2). When a H_2 molecule approaches a tetrahedrally distorted square-planar $Rh^{I}(bpy)_2^+$ complex, the two bpy ligands twist to form a five-coordinate geometry with the incoming H_2 (see Figure S6). The TS complex has C_2 symmetry and can be characterized as a dihydrogen-like complex. The dihydrido product exhibits a pseudo-octahedral geometry with the hydride ligands being nearly trans to the N−Rh bonds (Figure 5, bottom right).

A possible reason for the smaller activation volume associated with oxidative addition of H_2 in the Rh system than that in the case of $IrCl(CO)(PPh_3)_2$ may be the influence of the bulky bipyridine ligands that dominate the partial molar volumes of the Rh complexes, while dihydrogen and dihydride are comparatively small ligands. Thus, the transition state that includes the dihydrogen within the inner coordination sphere of the Rh complex (i.e., within the arms of the bpy ligands) would have a volume that is insensitive to the actual Rh−H or H−H distances. As a consequence, the volume of the TS and the product would be similar and account for the near equality in the reaction and activation volumes for the forward reaction and the practically zero activation volume observed for the reverse reductive elimination process.

We can calculate the displacement volumes assuming that the molecules are tumbling in solution and that they occupy a spherical cavity defined by their longest axis. Using the longest H-to-H distances of $Rh^{I}(bpy)_2^+$ (11.57 Å), $Rh^{III}(H)_2(bpy)_2^+$ (11.88 Å), and the transition-state complex (11.87 Å) and adding 2.4 Å for the van der Waals radii of two H atoms,[35] the displacement volumes are calculated as 1430, 1525, and 1521 Å^3, respectively. The displacement volumes of the transition-state dihydrogen complex and the dihydrido product $Rh^{III}(H)_2(bpy)_2^+$ are indeed very similar, as suggested above. Thus, the activation and reaction volumes should be very similar, as is observed. We do not estimate the reaction volume since the displacement volume for dihydrogen, for which a single solvation shell would greatly affect the effective volume, would not be a reliable estimate of its contribution to ΔV^0. Furthermore, the possible existence of a solvent-bound five- (or six-)coordinate Rh reactant complicates estimates of the reaction volume.

(35) *CRC Handbook of Chemistry and Physics*, 70th ed.; CRC Press: Boca Raton, FL, 1989.

The stability of the dihydrido complex is not significantly dependent on the polarity of the solvent. In the case of the Ir and Rh systems, the volume of activation was found to be insensitive to solvent (DMF, chlorobenzene, and toluene for the Ir system and acetone and methanol for the Rh system). This suggests that the polarity of the transition state is similar to that of the reactant.

The above discussion also allows us to understand the enthalpy and entropy profiles. The TS complex has a partially broken H−H bond and only a very weak partially formed Rh−H bond. Thus, the transition state does not energetically resemble either the reactants or products and is at higher energy than either of them. However, in entropic terms, the situation is much different. The H_2 has entered into the inner coordination sphere of the Rh complex and is shielded from the solvent by the large, slightly distorted bipyridine ligands, so the TS complex is entropically quite similar to the products, indicating a late transition state. As a consequence, the reaction and activation entropy for the forward reactions are very similar, as observed.

Acknowledgment. We thank Percefoni Doufou, Hideo Konno, and Mohamed S. A. Hamza for obtaining preliminary data. R.v.E. and M.S.A.H. gratefully acknowledge financial support from the Deutsche Forschungsgemeinschaft and the Alexander von Humboldt Foundation. X-ray data collection was performed with help of Dr. Jonathan Hanson at Beam Line X7B of the National Synchrotron Light Source at Brookhaven National Laboratory. This work was performed at BNL, funded under contract DE-AC02-98CH10886 with the U.S. Department of Energy and supported by its Division of Chemical Sciences, Office of Basic Energy Sciences.

Note Added after ASAP Publication. This article was released ASAP on January 5, 2006, with an incorrectly placed bracket in the numerator of eq 3 and an incorrect sign in the seventh line of the Electronic Structure Calculations section. The correct version was posted on January 11, 2006.

Supporting Information Available: Crystal data and structure refinement, and other X-ray crystallographic data in CIF format; conversion of standard states; DFT-optimized Cartesian coordinates for $Rh^{I}(bpy)_2^+$, $Rh^{III}(H)_2(bpy)_2^+$, and the transition-state complex; complete bond distances and angles for $Rh^{III}(H)_2(bpy)_2^+$ and the transition-state complex; plot of rate constants for formation of $Rh^{III}(H)_2(bpy)_2^+$ as a function of $[H_2]$; plots for the determination of activation parameters; an ORTEP drawing and a packing diagram of $Rh^{I}(bpy)_2^+$; and two views of the transition-state complex. This material is available free of charge via the Internet at http://pubs.acs.org.

IC0515498